Journal of Materials Chemistry

Cite this: *J. Mater. Chem.*, 2011, **21**, 6854

www.rsc.org/materials

PAPER

An investigation into the effect of thickness of titanium dioxide and gold–silver nanoparticle titanium dioxide composite thin-films on photocatalytic activity and photo-induced oxygen production in a sacrificial system†

Sujata Kundu,[a] Andreas Kafizas,[a] Geoffrey Hyett,[a] Andrew Mills,[b] Jawwad A. Darr[a] and Ivan P. Parkin*[a]

Received 15th October 2010, Accepted 11th March 2011
DOI: 10.1039/c0jm03492d

Thin films of titanium dioxide and titanium dioxide with incorporated gold and silver nanoparticles were deposited onto glass microscope slides, steel and titanium foil coupons by two sol–gel dip-coating methods. The film's photocatalytic activity and ability to evolve oxygen in a sacrificial solution were assessed. It was found that photocatalytic activity increased with film thickness (from 50 to 500 nm thick samples) for the photocatalytic degradation of methylene blue in solution and resazurin redox dye in an intelligent ink dye deposited on the surface. Contrastingly, an optimum film thickness of ~200 nm for both composite and pure films of titanium dioxide was found for water oxidation, using persulfate ($S_2O_8^{2-}$) as a sacrificial electron acceptor. The nanoparticle composite films showed significantly higher activity in oxygen evolution studies compared with plain TiO_2 films.

1. Introduction

The use of titanium dioxide for semiconductor sensitized photocatalysis and water splitting processes is a key topic of interest in materials science.[1] It was initially brought to prominence by Fujishima *et al.*[2] who showed how UV excited titania could induce hydrogen production in a chemically biased system.[3,4] A lot of subsequent research focussed on making this process function with sunlight rather than solely UV light for applications in clean hydrogen fuel energy formation, with a broad range of semiconductors tested. However, the search still continues in finding a method of sustainably producing hydrogen fuel from the sunlight induced photochemically splitting water with high conversion efficiency and commercially viable cost.[5–13] The bulk of this research has focused on titanium dioxide as the semiconductor catalyst, due primarily to the position of its conduction and valence bands in relation to the redox potentials for water reduction and oxidation respectively. The robust physical, chemical and photochemical stability to numerous reaction cycles makes TiO_2 an even more attractive candidate for commercial application.[14–18] Nonetheless, the energy required to photo-excite titanium dioxide (3.0–3.2 eV, rutile/anatase phase) lies in the UV portion of the electromagnetic spectrum, representing just a fraction of the energy in sunlight (~4% at sea level). As a more significant portion of sunlight lies in the visible region of the electromagnetic spectrum (~43% at sea level) researchers have investigated alternative materials that command both suitable reduction potentials in addition to low energy band gaps. Materials such as CdS (2.43 eV) and CdSe (1.73 eV) have been proven to meet such requirements; however, high propensities to photo-corrode make these materials poorer candidates for long-lasting commercial applications than TiO_2.[19–21] Great interest has therefore been undertaken in making titania based catalysts better suited for sunlight water-splitting; one method being noble-metal composite formation.

There is also great interest in using titanium dioxide for self-cleaning surface applications.[1,4,22] This research has been applied commercially in the production of self-cleaning windows, Pilkington Activ™ for example[23] that is photo-activated using sub-385 nm radiation.[24] This titania coated glass exhibits both photocatalytic and photo-induced super-hydrophilic properties when photo-excited; photo-mineralising the organic surface grime and forming a super-hydrophilic surface that encourages water sheeting.[25,26] One method of improving the photocatalytic ability of TiO_2 is by metal/metal oxide doping.[27–30] Some studies have shown that the surface loading of noble metal nanoparticles onto the surface of semiconductors can also enhance the photocatalytic activity. It is understood that the noble metal particles act as a reservoir or trap for photo-generated electrons and mediates their interaction with the relevant surface absorbed electron acceptor (such as oxygen in the photo-mineralisation of organics).[18,31]

In this paper we report the sol–gel synthesis of a TiO_2 composite embedded with Ag and Au nanoparticles. We present

[a]*UCL Materials Chemistry Centre, Christopher Ingold Laboratories, Department of Chemistry, University College London, 20 Gordon Street, London, WC1H 0AJ, UK. E-mail: i.p.parkin@ucl.ac.uk; Fax: +44 20 7679 7463; Tel: +44 20 7679 4669*
[b]*Department of Pure and Applied Chemistry, University of Strathclyde Glasgow, 16 Richmond Street, Glasgow, G1 1XQ, UK*
† Electronic supplementary information (ESI) available. See DOI: 10.1039/c0jm03492d

the novel synthesis of this material on titanium foil and steel coupons for use as photo-diodes in the photo-driven oxidation of water (with a persulfate bias). Films were also deposited on glass, and tested for the photocatalytic activity against methylene blue in an aqueous environment and the photo-reduction of a resazurin based ink coating. A range of films with varying thicknesses were achieved by either modifying the withdrawal rate of substrates when dip-coated in the sol–gel or by dipping and annealing for several cycles. Pure TiO_2 standards were formed analogously; so that the possible improvement of the photocatalytic and water splitting properties in the composite films could be compared. To our knowledge this is the first photocatalytic water splitting study in which the metal catalyst particles have been created at the same time as the sol–gel film in a one pot synthesis. It is also the first study of the effect of film thickness on the efficiency of both photo-degradation and oxygen evolution from water from an identical set of films. Interestingly, it was found that films which were most effective in photo-oxidising water were not the most effective photocatalysts. In fact, an optimum film thickness was discovered for water photo-oxidation (~200 nm) and was explained by relating the photo-generated electron diffusion length to vectorial charge separation.

2. Experimental

All of the chemicals used were purchased from Sigma–Aldrich Chemical Co. The grades used were 99.5% propan-2-ol, 99.8% butan-1-ol, 99% methanol, 99% acetylacetone, 99% acetonitrile, 99% silver nitrate, 99.9% hydrogen tetra-chloroaurate(III) hydrate (auric acid), 98% tri-basic ammonium citrate, 97% titanium(IV) *n*-butoxide, and methylene blue solution 1% w/v. Ready cleaned and polished low iron content microscope slides (76 × 26 mm) were purchased from BDH. 0.5 mm thick steel sheets were supplied by Corus that were cut into 25 × 25 mm coupons. 0.1 mm thick 99.6% Ti foil coupons (25 × 25 mm) were purchased from Goodfellows.

2.1 Sol–gel synthesis

2.1.1 Synthesis of titanium dioxide precursor sol. Titanium *n*-butoxide (17.08 g) was chelated with a mixture of acetylacetone (2.51 g) and butan-1-ol (32 cm^3), and stirred for 1 hour at room temperature. The sol changed from colourless to a clear, golden yellow during the first hour of stirring. After stirring for an hour, the titanium *n*-butoxide precursor was hydrolysed by adding distilled water (3.66 g) dissolved in propan-1-ol (9.04 g) and stirred for a further hour. The colour of the solution slightly intensified to a dark orange in the second hour of stirring. Finally, acetonitrile (1.66 g) was added to the solution, and stirred for one more hour, before being allowed to stand and age overnight.

2.1.2 Synthesis of nanoparticle composite titanium dioxide precursor sol. The gold nanoparticles were made by the Turkevich method.[32] Auric acid (0.2063 g) was dissolved in distilled water (25 cm^3). Separately, tri-basic ammonium citrate (0.30 g) was dissolved in distilled water (25 cm^3). Distilled water (17 cm^3) was heated in a separate vessel. An aliquot (1.0 cm^3) of the auric acid solution was added to the distilled water when at 60 °C. The water was further heated until boiling, whereupon an aliquot (2.0 cm^3) of the citrate solution was added drop-wise to the boiling solution over a 1 min period. The solution changed from pale golden to dark blue, indicating the formation of the nanoparticle colloid. The solution was heated for a further 2 min before being allowed to cool to room temperature. Once cooled, the suspension (3.0 cm^3) was diluted with propan-2-ol (9.03 g) and added to the initial solution of titanium precursor sol (as prepared in Section 2.1.1) to create a Au–titania sol precursor solution. The solution was stirred for one more hour, then silver nitrate (0.852 g) dissolved in acetonitrile (2.89 g) was added to the sol, before leaving the solution to stir for a further hour, and allowing the sol to stand and age overnight.

When the sol–gel solutions had aged overnight, three kinds of substrate were dip-coated: (i) microscope slides (25 mm × 75 mm), (ii) steel coupons (25 mm × 25 mm) and (iii) Ti foil coupons (25 mm × 25 mm).

2.2 Varying the thickness of films

All substrates were initially washed before coating: first in methanol followed by distilled water and finally with propan-2-ol. The substrates were then allowed to air-dry for 2 hours before being mounted for dip-coating. Substrates were dip-coated in two ways. The first series was made by varying the withdrawal rate of the immersed substrate from the sols. The withdrawal rates were varied from 2–600 cm min^{-1}. Substrates that were quickly withdrawn from the sol were significantly thicker than those withdrawn at slower speeds. After the films were deposited onto the three substrate types for a range of withdrawal rates they were annealed in a furnace, from room temperature to 550 °C. The temperature was held at 550 °C for an hour, before the furnace was turned off. The door remained closed as the samples were left to cool down to room temperature inside the furnace overnight. The second series of films were made by loading a number of coats. Substrates were dip-coated at a fixed withdrawal rate of 120 cm min^{-1} and then annealed at 550 °C for 10 minutes before cooling to room temperature and repeating the process. The number of coating-annealing cycles was varied to produce films with a range of thicknesses. All samples were annealed for 1 hour at 550 °C at the final coating.

The two series of films formed on steel, Ti foil and glass substrates showed a range of interference colours, indicating films of varying thicknesses were achieved. An example image of all the films formed on glass from the two sol–gel solutions, TiO_2 and *n*AuAg–TiO_2, is shown in Fig. 1.

2.3 Characterisation of films

Raman spectroscopy was carried out using a Renishaw Raman System 1000 equipped with a HeNe laser. X-Ray diffraction (XRD) analysis was conducted using a Bruker AXS D8 Discover. The mean crystallite size was determined from the degree of line broadening and application of the Shearer equation. Scanning electron microscopy (SEM) was performed on a Jeol JSM-6301F scanning electron microscope. Energy dispersive X-ray (EDX) studies were conducted on a Hitachi S570 and Wavelength dispersive X-ray (WDX) analyses were

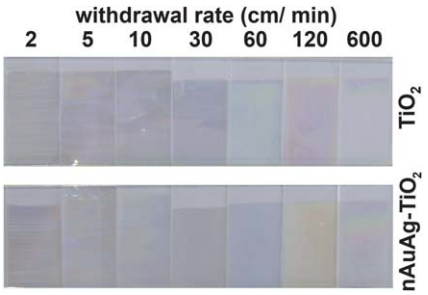

Fig. 1 Top down digital photograph of the array of TiO_2 and *n*AuAg–TiO_2 thin-films on glass made from System 1, where the withdrawal rate when dip-coated in the sol–gel was varied in order to achieve films of varying thicknesses. A range of interference colours were observed, indicative of varying thickness across both sets of films.

undertaken using a Philips ESEM. UV-visible spectroscopy was carried out using a PerkinElmer Lambda 25 UV/VIS spectrometer. The 254 nm UVC and 365 nm UVA irradiation were supplied from Vilber Lourmat VL-208G 8W and VL-208BLB 8W lamps respectively. From a distance of 15 cm, the lamp powers were 1 800 μW cm^{-2} for the 254 nm lamp and 1 300 μW cm^{-2} for the 365 nm lamp.

2.4 Functional characterisation of films

2.3.1 Water droplet contact angle change in UV light. From the second series of films, whereby a number of dip-coats and calcinations were applied in forming thicker films; the three 20 coat *n*AuAg–TiO_2 films on glass, steel and titanium were assessed. All samples were initially irradiated with 254 nm UVC light for 1 hour to ensure that any organic contaminant on the sample surface was degraded. Samples were then placed in the dark for 72 hours in order to allow the surface to revert to its initial hydrophobic state. A 1 μl water droplet was then placed on the surface of the film and the diameter of the spread measured. The sample was irradiated with 365 nm UVA light for a set period of time, before a fresh droplet was applied to the surface and measured. This testing process was repeated at regular intervals over 2 hours. The contact angle the droplet made with the surface was then calculated computationally from the measured spreads.[25]

2.3.2 Electrical conductivity. This was measured using a two-point probe. The two probes were held 2 mm apart at an approximate 45° angle to the surface. The coating on glass was highly resistive, and beyond the capacity of the probe to be measured. However, the coatings on steel and Ti foil both showed electrical conductivity. This was explained by current leaking through shrink-cracks formed in the film through annealing that penetrated through to the conductive metal substrates.

2.3.3 Methylene blue dye cell test. The quantitative rate of photocatalysis of samples was assessed by measuring the photocatalytic degradation (molecules destroyed cm^{-2} s^{-1}) of methylene blue solution (MB).[33,41] From the second series of films, the 2 coat *n*AuAg–TiO_2 films on steel and titanium substrates were tested, in addition to a commercially available standard, Pilkington Activ™ glass. The samples were placed in direct contact with a MB solution of fixed volume (4.0 ml) and concentration (1 μM). After equilibration, samples were exposed to 365 nm UVA light to induce photocatalysis. The change in MB concentration was measured at regular intervals using UV-visible spectroscopy, and the degradation rate determined. Notably the solution was continuously stirred whilst irradiated.

2.3.4 Resazurin intelligent ink test. The photocatalytic activity of the films was also qualitatively measured using a resazurin-based intelligent ink.[42,43] The first series of films, dip-coated on glass with various withdrawal speeds, were arranged in the order of thickness when mounted onto glass supports. The intelligent ink was then spray-coated evenly over the surface of the thin-films. The arrays were subsequently irradiated under 365 nm UVA light in-between regular intervals of flat-bed digital scanning. As the photocatalyst photo-reduced the redox dye in the intelligent ink from resazurin to resorufin to bleached intermediates, the ink changed colour from royal blue to pink to colourless. The time taken for the colour changes to occur, quantified by a colour extraction program, indicated the relative photoactivity of the films. If a film rapidly turned the ink pink and then colourless, it was highly photoactive, and if it took longer, it was less photoactive.

2.3.5 Oxygen evolution studies. To test the potential application of these films in water splitting devices, one half of the splitting reaction was examined, the oxidation of oxygen anions to the gas. An aqueous sacrificial solution consisting of 0.1 M NaOH and 0.01 M $Na_2S_2O_8$ was used. The change in voltage was measured using a Rank Brothers electrode system.[44] By initially purging the system with O_2, and then N_2 gas, the voltages for purely saturated (maximum oxygenated water) and unsaturated (zero oxygen water) solutions were measured. When the photocatalyst was excited by 365 nm UVA light, O_2 formed and induced a change in measured voltage. The changes in voltage during the photo-reaction could then relate to rates of oxygen evolution, as the voltage increased towards saturation (where the level of water saturated by O_2 is known to be 40 mg L^{-1} at 298 K, 1 atm). For a blank test, no change in voltage was observed. Any change in voltage was attributed solely to the photocatalytic evolution of O_2 from the aqueous sacrificial solution. To aid the water splitting process, all samples were sputtered with Pt on the reverse side of the sample (the side not irradiated with UVA light). This enhanced the rate of oxygen formation and was explained by more efficient charge separation of photo-excitations and reduction of the sacrificial electron acceptor (SEA) at Pt sites. A comparative experiment for a reverse Pt sputtered film and non-sputtered film showed that the increase of water oxidation increased by a factor of four.

3 Results and discussion

3.1 Film synthesis and characterisation

Two series of films were made by a sol–gel dip coating process of two sols, titanium dioxide (TiO_2) and titanium dioxide embedded with silver/gold nanoparticles (herein denoted *n*AuAg–TiO_2). The two series of each film type were made by either (i) varying

the withdrawal speed of the substrate from solution from 2–600 cm min^{-1} and annealing (System 1) or (ii) dipping and annealing for a number cycles at a constant withdrawal speed (System 2). Three different types of substrate were coated: glass, steel and titanium foil. The films showed interference colours due to variations in film thickness, as shown in Fig. 1.

3.1.1 Raman spectroscopy. Raman spectroscopy showed the sole presence of titania in all the films synthesised in this study. Fig. 2 shows an example Raman spectrum for a 5 coat *n*AuAg–TiO_2 film on Ti foil (System 2). A prominent peak at 144 cm^{-1} with additional smaller peaks at 197 cm^{-1}, 320 cm^{-1}, 399 cm^{-1} and 515 cm^{-1} related to the anatase phase and peaks at 245 cm^{-1}, 357 cm^{-1} and 560 cm^{-1} were attributed to the presence of rutile, labelled A = anatase and R = rutile in Fig. 2. The anatase peaks were far more intense than those of rutile. For *n*AuAg–TiO_2 thin-films, a separate gold or silver metallic/oxide phase was not observed. Given their notoriety as poor Raman scatterers, their presence was not expected to be observed by this method, especially given their low concentrations in the original sol–gel.

By comparing the relative intensities of anatase and rutile peaks for all films, a similar ratio was consistently observed, whether composite or pure TiO_2 and across the range of thicknesses. A quantitative indication of the relative concentrations of the two phases can be calculated from comparisons with pre-formulated anatase–rutile powders.[34] The anatase : rutile ratio was thus determined to be ~3 : 1 for all films made in this study. It has also been demonstrated that peak broadening in Raman spectra indicates the degree of crystallinity, where sharper peaks arise from larger crystallites.[46] No significant variation in the peak widths observed for samples deposited by System 1 (varied withdrawal rate) when compared to System 2 (several cycles of dip-coats and annealing stages at a constant withdrawal rate). This showed that the brief annealing stage (10 min) for samples made by System 2 did not alter the overall crystallinity of films.

3.1.2 X-Ray diffraction, XRD. All films made in this study were confirmed to be titania by XRD analysis. Both peaks relating to anatase ($I4_1/amdz$, $a = 3.782$ Å, $c = 9.504$ Å) and rutile ($P4_2/mnm$, $a = 4.624$ Å, $c = 2.984$ Å) phases were observed. No separate phases for the gold or silver nanoparticles embedded within *n*AuAg–TiO_2 thin-films were observed. Given their low concentration, in addition to the low particle diameters, it was likely that any presence would be swamped by peaks relating to the host titania matrix.

Fig. 3 shows the XRD pattern of *n*AuAg–TiO_2 deposited on Ti foil at a withdrawal rate of 120 cm^{-1}. Peaks labelled A and R describe anatase and rutile diffractions respectively. From the relative intensities of each phase, the ratio of anatase : rutile was estimated to be 2 : 1. Peaks labelled Ti are due to diffractions from the underlying titanium foil substrate.

The crystallite size as assessed from line broadening was very consistent across films of different thicknesses, and also across the range of substrates used and noted to be *ca.* 400 Å from Scherrer calculations. No significant increase in the degree of crystallinity for samples was seen for samples made from System 2, where repeated calcinations took place. As annealing stages never increased above a 550 °C threshold, the consistency in crystallinity was not surprising, where previously temperatures greater than 650 °C were required for appreciable increases in crystallinity to be observed.[47] Combining Raman and XRD evidence, any observed enhancement in the functional properties tested could not be attributed to changes in crystallinity. Interestingly, the chemical vapour deposition (CVD) growth of titanium dioxide on titania foil was shown to have a strong surface directing effect, resulting in the growth of films that are predominantly in the rutile phase of TiO_2.[35–39] The sol–gel synthesis used in this study resulted in a mixture of anatase and rutile phases, with the majority of the film forming the anatase phase.

3.1.3 Scanning electron microscopy, SEM. SEM images of the TiO_2 and *n*AuAg–TiO_2 films were taken for all three substrate coatings. The samples were viewed at high resolution from both top and side. Under high magnification, samples were generally flat and uniform with the exception of shrink cracking, inherent of sol–gel annealed thin-films. Example images are displayed in Fig. 4 of a *n*AuAg–TiO_2 sample withdrawn at a rate of 120 cm min^{-1} (System 1) at successive magnifications.

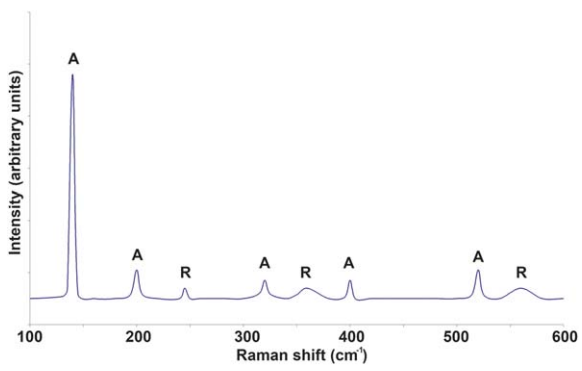

Fig. 2 Raman spectrum of a 5 coat *n*AuAg–TiO_2 sample deposited on titanium foil made from System 2, involving 5 cycles of dip-coats and annealing stages. Labels A and R correspond to anatase and rutile vibrational modes respectively.

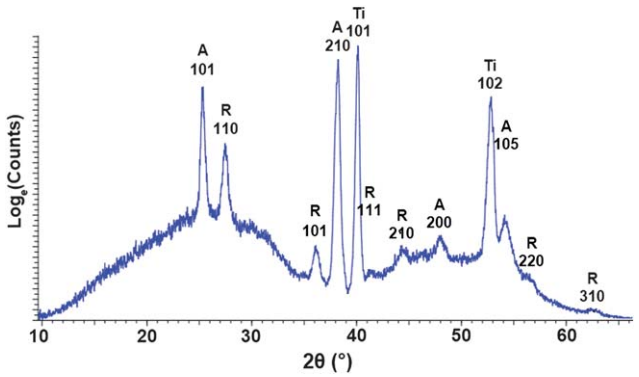

Fig. 3 XRD diffraction pattern for *n*AuAg–TiO_2 deposited on titanium foil at a withdrawal rate of 120 cm min^{-1} (System 1). Peaks labelled A and R represent diffractions from anatase and rutile phases respectively. Peaks labelled Ti represent diffractions from the underlying titanium foil substrate.

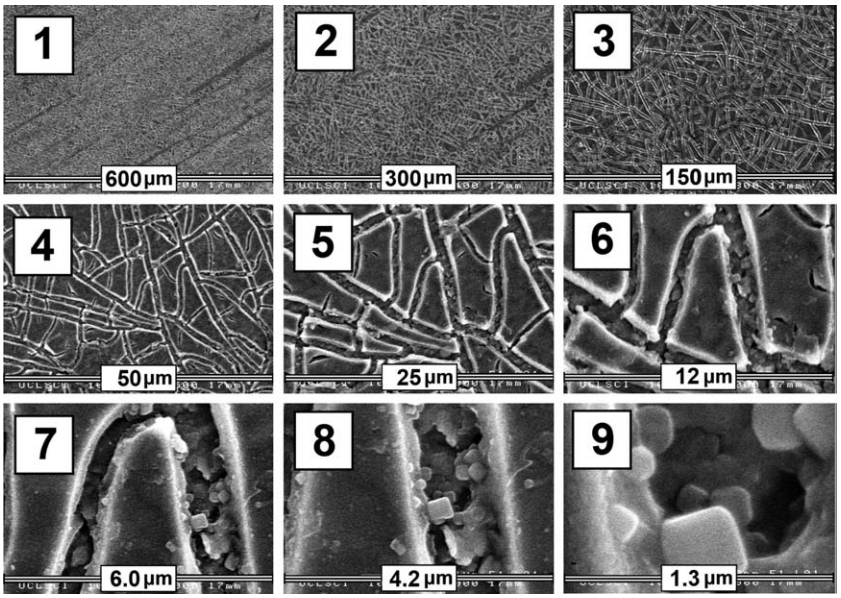

Fig. 4 SEM images of *n*AuAg–TiO_2 deposited on titanium foil at a withdrawal rate of 120 cm min^{-1} (System 1). Images show the film at successive magnifications where 1 = 200×, 2 = 400×, 3 = 800×, 4 = 2 500×, 5 = 5000×, 6 = 10 000×, 7 = 20 000×, 8 = 30 000×, 9 = 100 000× magnification. The scale-bars indicate the width of each image in microns.

Side on SEM was carried out on the same film, and can be seen in Fig. 5. The bulk of each image towards the bottom right corner is the titanium foil substrate on which the film lies. Cracks were observed in top-down SEM images; however it appears that not all of the film fragments are entirely flat. Due to shrink cracking of the sol upon annealing, individual plates of film were formed on the surface. Some are curved at the edges, and not in total contact with the substrate. The same effect has been seen on samples of the same coating on microscope slides as well as steel coupons. This is likely due to significant difference in the thermal expansion coefficient between the metal oxide and the substrate.

Side-on SEM images were taken from a tilted position to determine the thickness of films. Fig. 6 shows four separate images taken from across the *n*AuAg–TiO_2 sample withdrawn at a rate of 120 cm min^{-1} (System 1) on titanium foil. Images 2–4 in fig. 6 display the very fine microstructure of the surface and edges of the plate-like structures. SEM showed the presence of bright spots throughout the film of ~1 micron or larger in *n*AuAg–TiO_2 films, corresponding to metal islands.

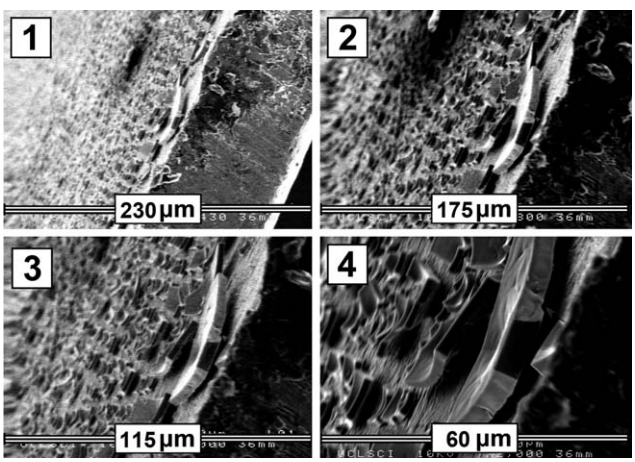

Fig. 5 Side on SEM images of *n*AuAg–TiO_2 deposited on titanium foil at a withdrawal rate of 120 cm min^{-1} (System 1). Images show the film side on where 1 = 430×, 2 = 800×, 3 = 1 000×, 4 = 2 000× magnification. The scale-bars indicate the width of each image in microns.

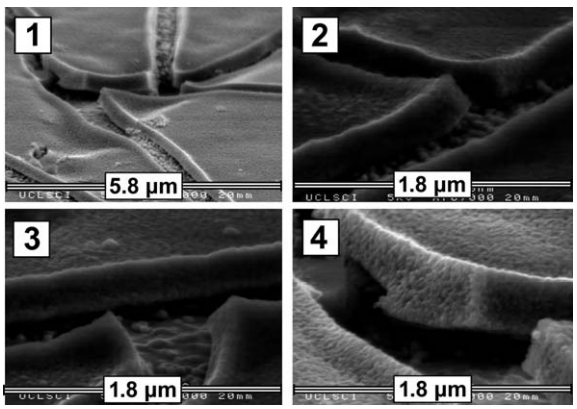

Fig. 6 Tilted SEM images of *n*AuAg–TiO_2 deposited on titanium foil at a withdrawal rate of 120 cm min^{-1} (System 1). Images show the film tilted where 1 = 20 000× and 2, 3, 4 = 70 000× magnification. The scale-bars indicate the width of each image in microns.

3.1.4 Energy-dispersive X-ray analysis, EDX. EDX was used to analyse the composition of the thin-films produced on all substrates. The results shown in Fig. 7 represent a *n*AuAg–TiO_2 sample withdrawn at a rate of 120 cm min^{-1} (System 1) on a steel coupon. First, the film was analysed over a wide area to identify the average components within the film. The results normally show a composition mixture of the substrate and the thin-film coating as the EDX beam penetrates several microns deep into the sample. An image of an analysed area is shown (Fig. 7(a)), with the results identifying Fe and Cr within the steel substrate.

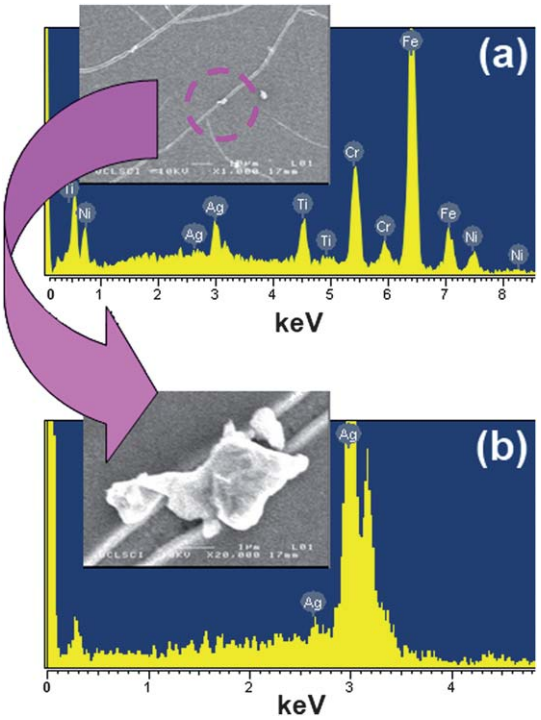

Fig. 7 EDX elemental analysis and the corresponding SEM images for (a) a wide area analysis and (b) a close up analysis of a silver agglomerate within a *n*AuAg–TiO_2 deposited on a steel coupon at a withdrawal rate of 120 cm min^{-1} (System 1).

The other major peaks were identified as Ti, Au and Ag. Taking a closer look at the film surface, silver agglomerates[27] were observed protruding from the smooth surface of the film (Fig. 7 (b)). These agglomerations were found regularly across the surface of all composite thin-films. It is thought that the enhancement in activity of the *n*AuAg–TiO_2 film, when compared with plain TiO_2, is due to the increased charge separation of the electrons and holes. As the metallic agglomerations act as reservoirs for electric charge, the rate of recombination of photo-generated species would be reduced.

3.1.5 Wavelength-dispersive X-ray diffraction, WDX. WDX analysis was performed on a sample of *n*AuAg–TiO_2 sample withdrawn at a rate of 120 cm min^{-1} (System 1) deposited on glass. Au was this time observed with an average concentration of 0.45 atom%. This was possibly not observed by EDX analysis due to the tendency for heavy peak overlap. Nevertheless, this level of detected gold was far below the 2 atom% inserted in the original sol. Similarly, Ag was observed at a similarly low concentration of 0.30 atom% incorporation. By analysing individual islands with WDX spot analysis, each metallic island was found to consist almost entirely of either silver or gold. The gold and silver islands did not form alloys. This was a consequence of the synthetic method where the Ag and Au nanoparticles were made independently and separately introduced into the sol.

3.1.6 Test for adhesion and robustness. All TiO_2 and *n*AuAg–TiO_2 films on all substrates were tested for their adhesion using the Scotch® tape test. All films of all thicknesses adhered well to the substrate, and were not removed. There was a little delamination on the trailing edges of the thickest films deposited onto microscope slides by System 1 (600 cm min^{-1} withdrawal rate), but the bulk of the film remained firmly stuck to the substrate. Nonetheless, the corresponding films on steel and titanium did not delaminate in this manner. All films were tested for robustness by scratch tests. All of the coatings were able to withstand being brushed with tissue, Wypall blue roll™, paper, brass and a steel scalpel; however, they were all easily scratched by a diamond pencil.

3.1.7 Water droplet contact angle change in UV light. The contact angle of a 1 μl water droplet placed on the surface of *n*AuAg–TiO_2 films (a withdrawal rate of 120 cm^{-1}—System 1) was measured for films deposited on glass, titanium and steel. The change in contact angle when exposed to 365 nm UVA irradiation was measured at regular intervals. A bar chart of the corresponding contact angles are shown in Fig. 8. It can be seen that all films displayed photo-induced superhydrophilicity,[25,26] as the contact angle reduces with increased UVA irradiations to below 5°. However, the film deposited on glass showed the most rapid transition to a super-hydrophilic state.

3.1.7 UV-visible spectroscopy. UV-visible spectroscopy was used to determine the thickness of films on glass and metals by analysing the interference patterns from transmittance/reflectance spectra. An example reflectance spectrum over the 200–2500 nm range is shown in Fig. 9 for a 2 coat *n*AuAg–TiO_2 film deposited on titanium (System 2).[40] The positions of maxima and minima were used in determining the film thickness by the Swanepoel method. In this instance, the thickness of the film formed from two cycles of dip-coating and annealing stages was determined to be 240 nm, which closely correlates to the thickness obtained by side-on SEM of ~250 nm. The thickness increased with multiple dip-coats or speed of substrate withdrawal from the sol (ESI†, Fig. S1 and S2 respectively) for all film types and substrates. The most constant increase in thickness was observed for System 2, the method in which the samples were annealed between repeated dips. These showed an aggregate increase in film thickness of ~120 nm per dip and anneal cycle. The process of varying the withdrawal rate enabled films from 40

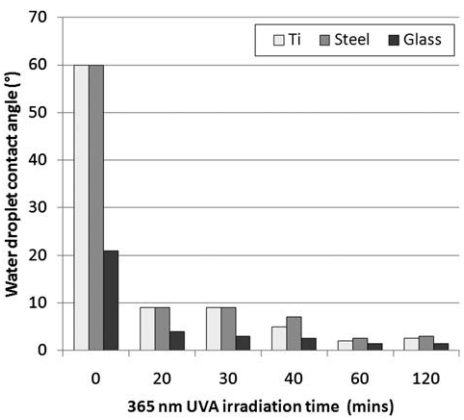

Fig. 8 Change in water droplet contact angle upon exposure to 365 nm UVA light for set irradiation periods for a *n*AuAg–TiO_2 film made at a withdrawal rate of 120 cm min^{-1} (System 1) on the three substrates: glass, titanium and steel.

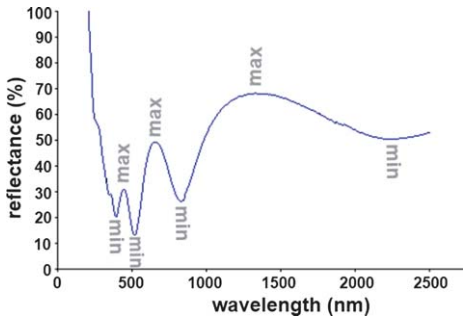

Fig. 9 UV-visible reflectance spectrum for a 2 coat *n*AuAg–TiO_2 thin-film deposited on titanium foil (System 2). The positions of the respective maxima and minima were used in deriving the thickness of the film through the Swanepoel method.

to 250 nm in thickness to be obtained. The film thickness was directly proportional to the withdrawal rate. Very similar trends in varying thickness were observed on steel and titanium coupons for each deposition method; however the thickness of films on the metal coupons was slightly greater than that of their respective glass deposited counterpart.

3.2 Tests for photocatalytic properties

3.2.1 Degradation of methylene blue. The 5 coat *n*AuAg–TiO_2 films deposited on steel and titanium (System 2) were tested against a commercially available standard Activ™ glass (TiO_2 anatase). The results are shown in Fig. 10. It was observed that Activ™ degraded methylene blue with a rate constant of 0.0016 s^{-1}. The coating on steel showed a marginally greater rate constant of 0.0022 s^{-1}; however the coating on titanium foil showed the most significant rate constant of 0.0071 s^{-1}. This showed the film on titanium foil was around four times more potent than Pilkington Activ™ in destroying methylene blue at UVA wavelengths.

3.2.2 Resazurin based intelligent ink test. The photocatalytic activity of the films was also qualitatively measured using a blue intelligent ink.[42] The experiment entailed the coating of films in an even layer of ink and monitoring the photo-induced reaction through a series of digital photographs. Fig. 11 shows a chronological series of images for both TiO_2 and *n*AuAg–TiO_2 thin-films made in System 1 (withdrawal rate variation). The slides at 0 min show the array (from thinnest to thickest—left to right) with a spray coated layer of intelligent ink. After 10 min irradiation, the second thickest film is already converting the resazurin redox dye within the ink (royal blue) to resorufin (pink). This remains the leader in fully converting the ink to bleached intermediates, with each consecutively thin-film following after some time. It is noted that the rate of thin-film photocatalysts is dependent on the film thickness. This is intuitive as a thicker film will absorb more light yielding a greater number of photo-excitations. In this experiment, a similar trend is observed whereby thicker films are more active. It is also worthy of note that glass blanks coated on each end of the array did not change colour for the duration of the entire photocatalysis experiment, indicating colour changes were due solely to the photocatalytic process as well as the UVA lone stability of the ink. When comparing the two sets of films, TiO_2 and *n*AuAg–TiO_2, we can see at 10 min irradiation the composite films are degrading the ink at a faster rate than their pure counterpart. For films coated at a withdrawal rate of 5 cm min^{-1} or more, this trend remained consistent for the remainder of the experiment, indicating the composite films were slightly more active photocatalysts.

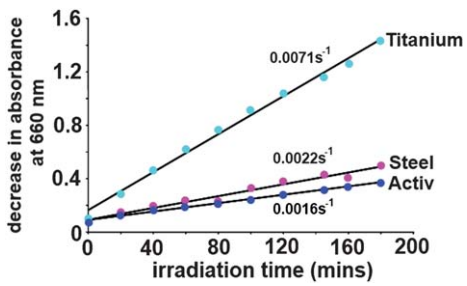

Fig. 10 Rate of degradation of methylene blue in solution for 5 coat *n*AuAg–TiO_2 films (System 2) deposited on steel and titanium, labelled Steel and titanium respectively. A commercial standard, Activ™ glass, was also tested, labelled Activ. The rate constant (s^{-1}) is quoted for each experiment.

Fig. 12 shows images of an analogous experiment; however this time performed of films made from System 2 (several dip-coats and annealing cycles). Films from 1–5 coats are tested for the two film types, TiO_2 and *n*AuAg–TiO_2. The thicker coatings again show a more active rate of photocatalysis than thinner coatings. However, the TiO_2 films degrade the ink slightly faster than the composite. It should be noted that the thickest films in this array (4 and 5 coats) took far less time to convert the ink layer pink and then colourless than any film from the array of System 1 made films. This was attributed to the fact that these thin-film coatings were nearly twice as thick (>400 nm) as the most active film in the System 1 array (~220 nm). The disparity in the activity of composite thin-films and doped thin films in these photocatalysis experiments was minimal. It was therefore concluded that the composite thin-films synthesised in this study were not conclusively any more active photocatalysts than plain anatase under UVA lighting.

3.3 Photo-oxidation of water—potential water splitting application

Initially, single coat TiO_2 and *n*AuAg–TiO_2 thin-films (System 2) deposited on glass, titanium and steel were tested for the photo-oxidation of water and liberation of O_2. It was found that films deposited on glass were unable to evolve significant levels of O_2; however films deposited on either of the metal substrates (titanium or steel) showed superior rates. The full ranges of thicknesses (System 1 and 2) were subsequently investigated for films deposited on all substrates: steel, titanium and glass. All samples were sputtered with Pt on the reverse side of substrates. Compared with pure TiO_2 films, *n*AuAg–TiO_2 proved to be a more active water photo-oxidant.

Fig. 13 shows the results of the water photo-oxidation tests against varying thicknesses for *n*AuAg–TiO_2 films deposited on the three substrates. Series A and B refer to Systems 2 and 1 respectively. From Fig. 13 one can see that films deposited on the titanium substrates produced the greatest levels of oxygen in each

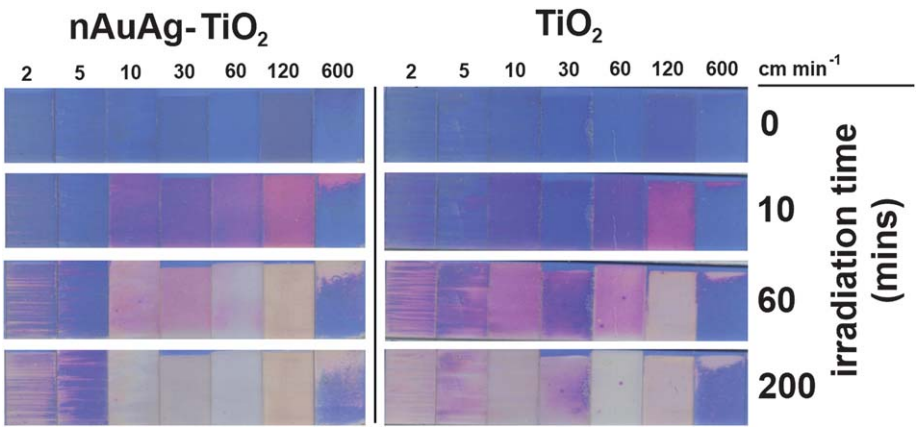

Fig. 11 A series of digital images of the photo-reduction of a resazurin based ink layer by 365 nm UVA light for both TiO_2 and *n*AuAg–TiO_2 film sets deposited by System 1. Film thickness increases from left to right, where a greater thickness purports a greater activity. Little variation in activity between TiO_2 and *n*AuAg–TiO_2 was observed.

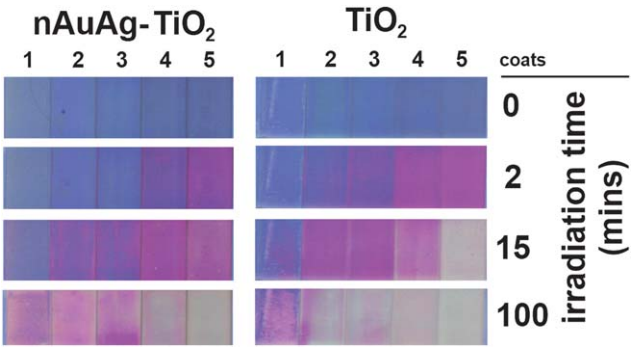

Fig. 12 A series of digital images of the photo-reduction of a resazurin based ink layer by 365 nm UVA light for both TiO_2 and *n*AuAg–TiO_2 film sets deposited by System 2. Film thickness increases from left to right, where a greater thickness purports a greater activity. Little variation in activity between TiO_2 and *n*AuAg–TiO_2 was observed.

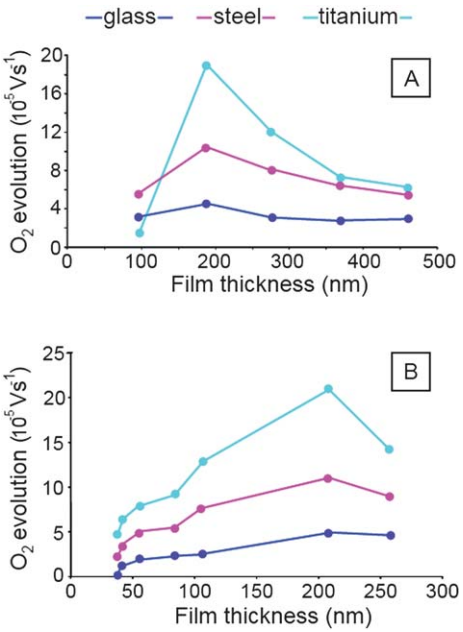

Fig. 13 Rate of O_2 evolution (10^{-5} V s^{-1}) in a sacrificial system *versus* film thickness for a set of *n*AuAg–TiO_2 films prepared by either (A) repeated cycles of dip-coats and annealing stages (System 2) or (B) varying the withdrawal rate from sol for a single dip-coat (System 1).

series across the board; with the exception of a steel substrate coated film of 100 nm thickness in System 1 (Fig. 13(B)). Both systems for making these films show an optimum thickness of approximately 200 nm where the highest levels of oxygen were produced. This is in contrast to photocatalysis studies (Fig. 11 and 12), where thicker films showed to be more active photocatalysts in the photo-reduction of resazurin dye. This shows us that the two processes, photocatalysis and photo-diode oxidation of water, operate through contrasting mechanisms, even though they are both reliant on initial photo-excitations to proceed.

Composite TiO_2 films embedded with gold and silver nanoparticles outperformed their corresponding pure TiO_2 counterpart when tested for the liberation of oxygen through the photo-oxidation of water. It is suggested that these embedded metal nanoparticles might act as electron reservoirs, decreasing the probability of a photo-generated electron to recombine with a photo-generated hole. As shown in the EDX image in Fig. 7, metallic islands were present in sol agglomerates, forming clusters on the cracked surface of composite films. It was previously suggested that the separate gold and silver islands dispersed throughout the material can better stabilise photo-excitations when acting in conjunction rather than alone.[48] It is also believed, due to the relatively high electronegativity of silver and gold compared to the TiO_2 bulk, photo-excited electrons are attracted to these metallic islands. The electrons held at these sites, away from concomitantly generated positive holes, inhibit electron–hole recombination and increase the efficiency of photocatalysis per photo-absorption.

Nonetheless, no significant increase in activity was observed between TiO_2 films and the composite in intelligent ink tests. This is because the intelligent ink functions *via* a mechanism in which photo-excited electrons reduce the redox dye. By placing an excess of glycerol within the ink as well, which acts as a sacrificial electron donor, photo-generated holes are scavenged. This in fact stabilises photo-excited electrons from recombining, encouraging the photo-reduction reaction process from occurring.

Given the ink system alone, in a sense, stabilises photo-excited electrons from recombining by scavenging holes; the mechanism by which gold and silver nanoparticles stabilise photo-excited electrons would not create as substantial a benefit. It can therefore be concluded that for the intelligent ink system, any benefit in photo-excited charge stabilisation would be significantly reduced; yielding the similar photocatalytic rates observed for *n*AuAg–TiO_2 and TiO_2 films tested in this study.

Further photocatalysis results show that the thickest films had the greatest propensity to photo-degrade the resazurin dye. This was simply attributed to the fact that thicker films absorb a greater portion of incoming light, thereby generating a greater number of electrons and holes. However, a distinct optimum film thickness for the photo-oxidation of water in a sacrificial system was contrastingly observed. Both TiO_2 and *n*AuAg–TiO_2 systems showed that a thickness of ~200 nm film was the optimum for water oxidation. It is probable that the diffusion length of the photo-generated electron[45] is such that the activity of the photocatalyst is optimised at a film thickness of ~200 nm for the electron to reach the underlying substrate without recombination with a positive hole. The platinum sputtered on the reverse-side of the steel/titanium coupon increased the effectiveness of water-splitting four-fold. This was attributed to the metal acting as an electron sink, increasing the level of charge separation in photo-excitation processes and further hindering recombination. It is likely that the higher rate of O_2 evolution for the *n*AuAg–TiO_2 film is due to a further enhanced level of charge separation within the photocatalyst film (and not due to substrate effects) due to the presence of Ag and Au islands embedded throughout the film.

4. Conclusion

Titanium dioxide and composite titanium dioxide gold/silver nanoparticulate films of different thicknesses were created by sol–gel dip-coating using two different deposition methods on microscope slides, steel coupons and titanium foil coupons. All films displayed photo-induced superhydrophilicity under 365 nm UVA light. A trend for increasing photocatalytic activity with increasing film thickness was observed, where thicker films were better photocatalysts in both resazurin reduction and methylene blue oxidation reactions. Contrastingly, the ability of films to liberate O_2 from the photo-oxidation of water with a sacrificial persulfate bias showed that films of ~200 nm thickness consistently showed the highest rate. It is therefore proposed that titania based photo-diode systems require an optimum thickness level of ~200 nm for enhanced water-splitting capabilities. On the underside of metal (titanium/steel) coated substrates, photo-generated electrons can travel through the film to the substrate where reduction processes can occur. By platinising the substrate, a four-fold increase in activity was observed as the noble metal acted as a better electron sink. However, photo-excited electrons in thicker films would be required to travel a greater distance on average to the back end of the film; thereby making recombination processes more likely. Therefore, an optimum level where the best balance between the increased number of photo-absorptions due to increased film thickness and the short distance to the platinised reverse side was plausible. TiO_2 films embedded with silver and gold nanoparticles outperformed pure TiO_2 in the water photo-oxidation tests. The enhancement of activity of TiO_2 by the introduction of noble metal dopants can be explained in part by a charge separation model in which the clusters of silver and gold behave as electron reservoirs that further inhibit recombination processes from occurring and drive surface oxidation through protection of concomitant electron holes.

References

1 A. Mills and S. LeHunte, *J. Photochem. Photobiol., A*, 1997, **108**, 1.
2 S. Nakabayashi, A. Fujishima and K. Honda, *Chem. Phys. Lett.*, 1983, **102**, 464.
3 F. H. Sobrino, C. R. Monroy and J. L. H. Perez, *Renewable Sustainable Energy Rev.*, 2010, **14**, 772.
4 A. Fujishima, T. N. Rao and D. A. Tryk, *J. Photochem. Photobiol., C*, 2000, **1**, 1.
5 N. D. Uri, *Electr. Power Syst. Res.*, 1981, **4**, 247.
6 S. Shafiee and E. Topal, *Energ. Pol.*, 2009, **37**, 181.
7 M. I. Hoffert, K. Caldeira, G. Benford, D. R. Criswell, C. Green, H. Herzog, A. K. Jain, H. S. Kheshgi, K. S. Lackner, J. S. Lewis, H. D. Lightfoot, W. Manheimer, J. C. Mankins, M. E. Mauel, J. Perkins, M. E. Schlesinger, T. Volk and T. M. L. Wigley, *Science*, 2002, **298**, 981.
8 F. Barbir, T. N. Veziroglu and H. J. Plass, Jr, *Int. J. Hydrogen Energy*, 1990, **15**, 739.
9 J. M. Beér, *Prog. Energy Combust. Sci.*, 2000, **26**, 301.
10 S. Kaul and R. Edinger, *Energ. Pol.*, 2004, **32**, 929.
11 N. Hallale and F. Liu, *Adv. Environ. Res.*, 2001, **6**, 81.
12 J. S. Gaffney and N. A. Marley, *Atmos. Environ., Part A*, 1990, **24**, 3105.
13 B. Scrosati and J. Garche, *J. Power Sources*, 2010, **195**, 2419.
14 N. Meng, M. K. H. Leung, D. Y. C. Leung and K. Sumathy, *Renewable Sustainable Energy Rev.*, 2007, **11**, 401.
15 L. Meiying, Y. Wansheng, L. Zhibin, T. Takata, K. Domen and L. Can, *Chin. J. Catal.*, 2006, **27**, 556.
16 S. Licht, *Int. J. Hydrogen Energy*, 2005, **30**, 459.
17 A. Iwase, H. Kato and A. Kudo, *Catal. Lett.*, 2006, **108**, 7.
18 A. Galińska and J. Walendziewski, *Energy Fuels*, 2005, **19**, 1143.
19 J. K. Dohrmann and J. Reck, *J. Electroanal. Chem.*, 1998, **452**, 215.
20 F. Liangbo, W. Hanqing, J. Zhensheng, L. Qinglin and S. Mengyang, *J. Photochem. Photobiol., A*, 1991, **56**, 89.
21 L. Huang, F. Peng, H. Yu and H. Wang, *Solid State Sci.*, 2009, **11**, 129.
22 Y. Katsunori and M. Ishikawa, *Catal. Surv. Jpn.*, 2000, **4**, 83.
23 LaminatedGlassNews, http://www.dupont.com/safetyglass/lgn/stories/2208.html.
24 I. P. Parkin, A. Mills and A. Lepre, *J. Photochem. Photobiol., A*, 2003, **160**, 213.
25 J. C. Yu, J. Yu, W. Ho and J. Zhao, *J. Photochem. Photobiol., A*, 2002, **148**, 331.
26 A. Marmur, *Langmuir*, 2004, **20**, 3517.
27 K. Page, R. J. Palgrave, I. P. Parkin, M. Wilson, S. L. P. Savin and A. V. Chadwick, *J. Mater. Chem.*, 2007, **17**, 95.
28 S. D. Sharma, D. Singh and K. K. Saini, *Appl. Catal., A*, 2006, **314**, 40.
29 S. R. Sonawane and M. K. Dongare, *J. Mol. Catal. A: Chem.*, 2006, **243**, 68.
30 E. Celik, Z. Gokcen and N. F. A. Azem, *Mater. Sci. Eng., B*, 2006, **132**, 258.
31 D. Eder, M. Motta and A. H. Windle, *Nanotechnology*, 2009, **20**, 055602.
32 J. Kimling, M. Maier, B. Okenve, V. Kotaidis, H. Ballot and A. Plech, *J. Phys. Chem. B*, 2006, **110**, 15700.
33 P. Evans, S. Mantke, A. Mills, A. Robinson and D. W. Sheel, *J. Photochem. Photobiol., A*, 2007, **188**, 387.
34 A. Kafizas, C. Crick and I. P. Parkin, *J. Photochem. Photobiol., A*, 2010, **216**, 156–166.
35 A. Mills, G. Hill, S. Bhopal, I. P. Parkin and S. A. O'Neil, *J. Photochem. Photobiol., A*, 2003, **160**, 185.
36 G. Hyett, M. A. Green and I. P. Parkin, *J. Am. Chem. Soc.*, 2006, **128**, 12147.

37 G. Hyett, M. A. Green and I. P. Parkin, *J. Am. Chem. Soc.*, 2007, **129**, 15541.
38 A. Kafizas, I. P. Parkin, C. W. Dunnill and G. Hyett, *ECS Trans.*, 2009, **25**, 1239.
39 A. Kafizas, G. Hyett and I. P. Parkin, *J. Mater. Chem.*, 2009, **19**, 1399.
40 N. Barati, M. A. Faghihi Sani, H. Ghasemi, Z. Sadeghian and S. M. M. Mirhoseini, *Appl. Surf. Sci.*, 2009, **255**, 8328.
41 A. Mills and M. McFarlane, *Catal. Today*, 2007, **129**, 28.
42 A. Mills and M. McGrady, *J. Photochem. Photobiol., A*, 2008, **193**, 228.
43 A. Kafizas, A. Mills and I. P. Parkin, *Anal. Chim. Acta*, 2010, **663**, 69–76.
44 Rank Brothers Oxygen Electrode, rankbrothers.co.uk/download/digioxy.pdf, 10th January 2011.
45 J. P. Gonzalez-Vazquez, J. A. Anta and J. Bisquert, *J. Phys. Chem. C*, 2010, **114**, 8552.
46 K. R. Wu and C. H. Hung, *Appl. Surf. Sci.*, 2009, **256**, 1595–1603.
47 G. Hyett, M. Green and I. P. Parkin, *J. Am. Chem. Soc.*, 2006, **128**, 12147.
48 A. Kafizas, S. Kellici, J. A. Darr and I. P. Parkin, *J. Photochem. Photobiol., A*, 2009, **204**, 183.